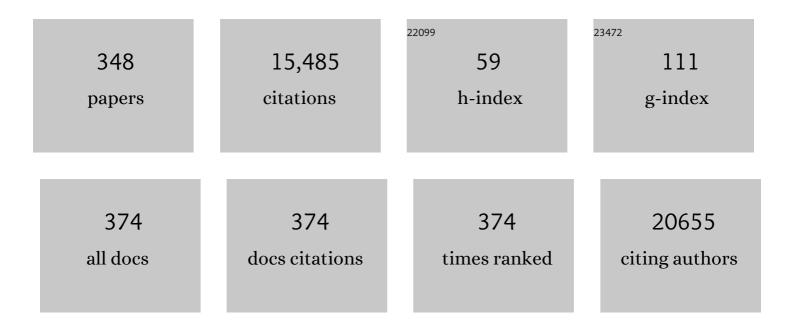
List of Publications by Year in descending order

Source: https://exaly.com/author-pdf/333511/publications.pdf Version: 2024-02-01



#	Article	IF	CITATIONS
1	Fine-tuning the cutpoint T-score as an epidemiological index with high specificity for osteoporosis: methodological considerations for the Chinese population. Quantitative Imaging in Medicine and Surgery, 2022, 12, 882-885.	1.1	7
2	â€~Healthier Chinese spine': an update of osteoporotic fractures in men (MrOS) and in women (MsOS) Hong Kong spine radiograph studies. Quantitative Imaging in Medicine and Surgery, 2022, 12, 2090-2105.	1.1	20
3	Fragility fracture prevalence among elderly Chinese is no more than half of that of elderly Caucasians. Quantitative Imaging in Medicine and Surgery, 2022, 12, 874-881.	1.1	14
4	Generalization Challenges in Drug-Resistant Tuberculosis Detection from Chest X-rays. Diagnostics, 2022, 12, 188.	1.3	11
5	A rapid deteriorated primary cerebellar Burkitt lymphomas with tiger-striped appearance. Japanese Journal of Clinical Oncology, 2022, , .	0.6	0
6	Further evidence supports a much lower prevalence of radiographic osteoporotic vertebral fracture in Hong Kong Chinese women than in Italian Caucasian women. Archives of Osteoporosis, 2022, 17, 13.	1.0	6
7	Spleen in viral Hepatitis-B liver fibrosis patients may have a reduced level of per unit micro-circulation: non-invasive diffusion MRI evidence with a surrogate marker. SLAS Technology, 2022, 27, 187-194.	1.0	5
8	Several concerns on grading lumbar disc degeneration on MR image with Pfirrmann criteria. Journal of Orthopaedic Translation, 2022, 32, 101-102.	1.9	4
9	Current Concepts in Imaging Diagnosis and Screening of Blunt Cerebrovascular Injuries. Tomography, 2022, 8, 402-413.	0.8	4
10	Osteoporotic vertebral endplate and/or cortex fracture is not always radiographically detectable. Osteoporosis International, 2022, , 1.	1.3	4
11	CT detects more osteoporotic endplate depressions than radiograph: a descriptive comparison of 76 vertebrae. Osteoporosis International, 2022, 33, 1569-1577.	1.3	9
12	Transforming a clinical fluorescent dye to sense and treat iron overload disorders: a new reverse translational approach in precision medicine. Quantitative Imaging in Medicine and Surgery, 2022, 12, 3020-3023.	1.1	1
13	Annotations of Lung Abnormalities in the Shenzhen Chest X-ray Dataset for Computer-Aided Screening of Pulmonary Diseases. Data, 2022, 7, 95.	1.2	6
14	Dietary cholesterol drives fatty liver-associated liver cancer by modulating gut microbiota and metabolites. Gut, 2021, 70, 761-774.	6.1	382
15	Age and gender dependence of liver diffusion parameters and the possibility that intravoxel incoherent motion modeling of the perfusion component is constrained by the diffusion component. NMR in Biomedicine, 2021, 34, e4449.	1.6	20
16	Interpretation of osteoporotic vertebral deformity on frontal view radiographs of the chest and abdomen: a pictorial review. Quantitative Imaging in Medicine and Surgery, 2021, 11, 423-442.	1.1	5
17	T1rho shortening effect of fat in liver steatosis after fat suppression: approximate estimation in a methionine and choline-deficient (MCD) diet rat model. Quantitative Imaging in Medicine and Surgery, 2021, 11, 870-875.	1.1	4
18	Observed paradoxical perfusion fraction elevation in steatotic liver: An example of intravoxel incoherent motion modeling of the perfusion component constrained by the diffusion component. NMR in Biomedicine, 2021, 34, e4488.	1.6	16

#	Article	IF	CITATIONS
19	Evidence of Tri-Exponential Decay for Liver Intravoxel Incoherent Motion MRI: A Review of Published Results and Limitations. Diagnostics, 2021, 11, 379.	1.3	18
20	Endoscopy-assisted magnetic navigation of biohybrid soft microrobots with rapid endoluminal delivery and imaging. Science Robotics, 2021, 6, .	9.9	164
21	Different tissue types display different signal intensities on <i>b</i> = 0 images and the implications of this for intravoxel incoherent motion analysis: Examples from liver MRI. NMR in Biomedicine, 2021, 34, e4522.	1.6	8
22	Illustration of a number of atypical computed tomography manifestations of active pulmonary tuberculosis. Quantitative Imaging in Medicine and Surgery, 2021, 11, 1651-1667.	1.1	5
23	Physiological variation of liver iron concentration may not be dominantly responsible for the liver T1rho variations associated with age and gender. Quantitative Imaging in Medicine and Surgery, 2021, 11, 1668-1673.	1.1	3
24	Improving osteoporotic vertebral deformity detection on chest frontal view radiograph by adjusted X-ray beam positioning. Journal of Orthopaedic Translation, 2021, 28, 169-178.	1.9	3
25	A reduction of perfusion can lead to an artificial elevation of slow diffusion measure: examples in acute brain ischemia MRI intravoxel incoherent motion studies. Annals of Translational Medicine, 2021, 9, 895-895.	0.7	9
26	Mutual constraining of slow component and fast component measures: some observations in liver IVIM imaging. Quantitative Imaging in Medicine and Surgery, 2021, 11, 2879-2887.	1.1	14
27	Citrate-Coated Magnetic Polyethyleneimine Composites for Plasmid DNA Delivery into Glioblastoma. Polymers, 2021, 13, 2228.	2.0	2
28	Gender-specific liver aging and magnetic resonance imaging. Quantitative Imaging in Medicine and Surgery, 2021, 11, 2893-2904.	1.1	8
29	More promising results of liver intravoxel incoherent motion imaging analysis for the assessment of nonalcoholic steatohepatitis and fibrosis. Annals of Translational Medicine, 2021, 9, 1283-1283.	0.7	1
30	Usefulness of diffusion derived vessel density computed from a simplified IVIM imaging protocol: An experimental study with rat biliary duct blockage induced liver fibrosis. Magnetic Resonance Imaging, 2021, 84, 115-123.	1.0	7
31	Diffusion-weighted MRI of the liver: challenges and some solutions for the quantification of apparent diffusion coefficient and intravoxel incoherent motion. American Journal of Nuclear Medicine and Molecular Imaging, 2021, 11, 107-142.	1.0	4
32	Much lower prevalence and severity of radiographic osteoporotic vertebral fracture in elderly Hong Kong Chinese women than in age-matched Rome Caucasian women: a cross-sectional study. Archives of Osteoporosis, 2021, 16, 174.	1.0	22
33	Association between cine CMR-based radiomics signature and microvascular obstruction in patients with ST-segment elevation myocardial infarction. Journal of Thoracic Disease, 2021, 14, 0-0.	0.6	3
34	Topically applied adipose-derived mesenchymal stem cell treatment in experimental focal cerebral ischemia. Journal of Clinical Neuroscience, 2020, 71, 226-233.	0.8	8
35	Underreporting characteristics of osteoporotic vertebral fracture in back pain clinic patients of a tertiary hospital in China. Journal of Orthopaedic Translation, 2020, 23, 152-158.	1.9	11
36	Chinese expert consensus on the diagnosis of osteoporosis by imaging and bone mineral density. Quantitative Imaging in Medicine and Surgery, 2020, 10, 2066-2077.	1.1	40

#	Article	IF	CITATIONS
37	Osteoporotic Vertebral Deformity: Radiological Appearances and Their Association With a History of Trauma and the Risk of Further Fragility Fracture. Canadian Association of Radiologists Journal, 2020, 72, 084653712095847.	1.1	9
38	Collagen deposition in the liver is strongly and positively associated with T1rho elongation while fat deposition is associated with T1rho shortening: an experimental study of methionine and choline-deficient (MCD) diet rat model. Quantitative Imaging in Medicine and Surgery, 2020, 10, 2307-2321.	1.1	16
39	Elderly men have much lower vertebral fracture risk than elderly women even at advanced age: the MrOS and MsOS (Hong Kong) year 14 follow-up radiology results. Archives of Osteoporosis, 2020, 15, 176.	1.0	19
40	Radiographic osteoporotic vertebral fractures in elderly men: a brief review focusing on differences between the sexes. Quantitative Imaging in Medicine and Surgery, 2020, 10, 1863-1876.	1.1	19
41	Diagnosis and grading of radiographic osteoporotic vertebral deformity by general radiologists after a brief self-learning period. Journal of Thoracic Disease, 2020, 12, 4702-4710.	0.6	7
42	Medical Imaging Engineering and Technology Branch of the Chinese Society of Biomedical Engineering expert consensus on the application of Emergency Mobile Cabin CT. Quantitative Imaging in Medicine and Surgery, 2020, 10, 2191-2207.	1.1	3
43	The role of radiography in the study of spinal disorders. Quantitative Imaging in Medicine and Surgery, 2020, 10, 2322-2355.	1.1	27
44	CT suggests discharged Covid-19 patients who were retested RT-PCR positive again for SARS-CoV-2 more likely had false negative RT-PCR tests before discharging. Quantitative Imaging in Medicine and Surgery, 2020, 10, 1396-1400.	1.1	5
45	Chest lesion CT radiological features and quantitative analysis in RT-PCR turned negative and clinical symptoms resolved COVID-19 patients. Quantitative Imaging in Medicine and Surgery, 2020, 10, 1307-1317.	1.1	17
46	Pre-treatment intravoxel incoherent motion diffusion-weighted imaging predicts treatment outcome in nasopharyngeal carcinoma. European Journal of Radiology, 2020, 129, 109127.	1.2	18
47	Recognizing osteoporotic vertebral deformity on frontal view radiograph: a cohort analysis and a pictorial review. Archives of Osteoporosis, 2020, 15, 41.	1.0	9
48	The role of CT for Covid-19 patient's management remains poorly defined. Annals of Translational Medicine, 2020, 8, 145-145.	0.7	46
49	The open access financial model hinders the growth of medical physics research in low―and middleâ€income countries. Medical Physics, 2020, 47, 5972-5975.	1.6	5
50	Pre-treatment amide proton transfer imaging predicts treatment outcome in nasopharyngeal carcinoma. European Radiology, 2020, 30, 6339-6347.	2.3	17
51	Existing severe osteoporotic vertebral fractures in elderly Chinese males were only weakly associated with higher further vertebral fracture risk at year-4 follow-up. Osteoporosis International, 2020, 31, 1593-1594.	1.3	9
52	Macromolecular proton fraction mapping based on spinâ€lock magnetic resonance imaging. Magnetic Resonance in Medicine, 2020, 84, 3157-3171.	1.9	6
53	Semi-quantitative grading and extended semi-quantitative grading for osteoporotic vertebral deformity: a radiographic image database for education and calibration. Annals of Translational Medicine, 2020, 8, 398-398.	0.7	31
54	A call for caution in extrapolating chest CT sensitivity for COVID-19 derived from hospital data to patients among general population. Quantitative Imaging in Medicine and Surgery, 2020, 10, 798-799.	1.1	17

#	Article	IF	CITATIONS
55	Diffusion MRI Derived per Area Vessel Density as a Surrogate Biomarker for Detecting Viral Hepatitis B-Induced Liver Fibrosis: A Proof-of-Concept Study. SLAS Technology, 2020, 25, 474-483.	1.0	21
56	Radiological features of traumatic vertebral endplate fracture: an analysis of 194 cases with 263 vertebral fractures. Chinese Medical Journal, 2020, 133, 2696-2702.	0.9	18
57	Dependence of intravoxel incoherent motion diffusion MR threshold <i>b</i> -value selection for separating perfusion and diffusion compartments and liver fibrosis diagnostic performance. Acta Radiologica, 2019, 60, 3-12.	0.5	19
58	Comparison of triâ€exponential decay versus biâ€exponential decay and full fitting versus segmented fitting for modeling liver intravoxel incoherent motion diffusion MRI. NMR in Biomedicine, 2019, 32, e4155.	1.6	25
59	Updates on 18F-FDG-PET/CT as a clinical tool for tuberculosis evaluation and therapeutic monitoring. Quantitative Imaging in Medicine and Surgery, 2019, 9, 1132-1146.	1.1	35
60	A modified semi-quantitative (mSQ) grading scheme for osteoporotic vertebral fracture in elderly women. Quantitative Imaging in Medicine and Surgery, 2019, 9, 146-150.	1.1	19
61	Elderly males with or without existing osteoporotic vertebral fracture have much lower future vertebral fracture risk than elderly females: the MrOS (Hong Kong) year-4 follow-up spine radiograph study. Osteoporosis International, 2019, 30, 2505-2514.	1.3	17
62	An update on PET-based molecular imaging in neuro-oncology: challenges and implementation for a precision medicine approach in cancer care. Quantitative Imaging in Medicine and Surgery, 2019, 9, 1597-1610.	1.1	26
63	Osteoporotic vertebral deformity with endplate/cortex fracture is associated with higher further vertebral fracture risk: the Ms. OS (Hong Kong) study results. Osteoporosis International, 2019, 30, 897-905.	1.3	49
64	Living tissue intravoxel incoherent motion (IVIM) diffusion MR analysis without b=0 image: an example for liver fibrosis evaluation. Quantitative Imaging in Medicine and Surgery, 2019, 9, 127-133.	1.1	27
65	Some radiographically â€~occult' osteoporotic vertebral fractures can be evidential if we look carefully. Quantitative Imaging in Medicine and Surgery, 2019, 9, 1992-1995.	1.1	13
66	On the possibility of over-diagnosis of osteoporotic vertebral fracture at mid-thoracic level. Journal of Thoracic Disease, 2019, 11, 5708-5711.	0.6	15
67	Topics on quantitative liver magnetic resonance imaging. Quantitative Imaging in Medicine and Surgery, 2019, 9, 1840-1890.	1.1	31
68	Amide proton transfer MRI detects early changes in nasopharyngeal carcinoma: providing a potential imaging marker for treatment response. European Archives of Oto-Rhino-Laryngology, 2019, 276, 505-512.	0.8	13
69	Osteoporotic Vertebral Fracture Prevalence in Elderly Chinese Men and Women: A Comparison of Endplate/Cortex Fracture–Based and Morphometrical Deformity–Based Methods. Journal of Clinical Densitometry, 2019, 22, 409-419.	0.5	38
70	High performance of intravoxel incoherent motion diffusion MRI in detecting viral hepatitis-b induced liver fibrosis. Annals of Translational Medicine, 2019, 7, 39-39.	0.7	24
71	MR imaging for acute pancreatitis: the current status of clinical applications. Annals of Translational Medicine, 2019, 7, 269-269.	0.7	27
72	Prevalence of cervical spine degenerative changes in elderly population and its weak association with aging, neck pain, and osteoporosis. Annals of Translational Medicine, 2019, 7, 486-486.	0.7	31

#	Article	IF	CITATIONS
73	Intravoxel incoherent motion derived liver perfusion/diffusion readouts can be reliable biomarker for the detection of viral hepatitis B induced liver fibrosis. Quantitative Imaging in Medicine and Surgery, 2019, 9, 371-371.	1.1	25
74	Removal of evidential motion-contaminated and poorly fitted image data improves IVIM diffusion MRI parameter scan–rescan reproducibility. Acta Radiologica, 2018, 59, 1157-1167.	0.5	23
75	MR imaging of hemorrhage associated with acute pancreatitis. Pancreatology, 2018, 18, 363-369.	0.5	18
76	No inferiority of Tonbridge thrombectomy device for acute thrombus retrial compared with Solitaire device: an experimental evaluation with a canine distal external carotid-maxillary artery occlusion model. Journal of NeuroInterventional Surgery, 2018, 10, 1085-1091.	2.0	10
77	Elderly population have a decreased aneurysmal subarachnoid hemorrhage incidence rate than Middle aged population: a descriptive analysis of 8,144 cases in mainland China. British Journal of Neurosurgery, 2018, 32, 165-171.	0.4	5
78	A Combined Use of Intravoxel Incoherent Motion MRI Parameters Can Differentiate Early-Stage Hepatitis-b Fibrotic Livers from Healthy Livers. SLAS Technology, 2018, 23, 259-268.	1.0	31
79	Breath-hold black-blood T1rho mapping improves liver T1rho quantification in healthy volunteers. Acta Radiologica, 2018, 59, 257-265.	0.5	13
80	Age- and Gender-Associated Liver Physiological T1rho Dynamics Demonstrated with a Clinically Applicable Single-Breathhold Acquisition. SLAS Technology, 2018, 23, 179-187.	1.0	15
81	Thoracolumbar Intervertebral Disc Area Morphometry in Elderly Chinese Men and Women. Spine, 2018, 43, E607-E614.	1.0	15
82	Senile osteoporosis is associated with disc degeneration. Quantitative Imaging in Medicine and Surgery, 2018, 8, 551-556.	1.1	23
83	Functional probes for cardiovascular molecular imaging. Quantitative Imaging in Medicine and Surgery, 2018, 8, 838-852.	1.1	14
84	Orthopaedic imaging for translational research and clinical application. Journal of Orthopaedic Translation, 2018, 15, A1-A2.	1.9	2
85	Osteoporotic vertebral endplate and cortex fractures: A pictorial review. Journal of Orthopaedic Translation, 2018, 15, 35-49.	1.9	36
86	Informed appropriate imaging for low back pain management: A narrative review. Journal of Orthopaedic Translation, 2018, 15, 21-34.	1.9	38
87	Appropriate Normal Range of Lumbar Disc T1rho of Men and Women with Respect to Physiological Aging. RoFo Fortschritte Auf Dem Gebiet Der Rontgenstrahlen Und Der Bildgebenden Verfahren, 2018, 190, 560-560.	0.7	1
88	SCOPE: signal compensation for low-rank plus sparse matrix decomposition for fast parameter mapping. Physics in Medicine and Biology, 2018, 63, 185009.	1.6	15
89	Radiological signs associated with pulmonary multi-drug resistant tuberculosis: an analysis of published evidences. Quantitative Imaging in Medicine and Surgery, 2018, 8, 161-173.	1.1	48
90	All osteoporotically deformed vertebrae with >34% height loss have radiographically identifiable endplate/cortex fracture. Journal of Orthopaedic Translation, 2018, 14, 63-66.	1.9	26

#	Article	IF	CITATIONS
91	Head and Neck Tumors: Amide Proton Transfer MRI. Radiology, 2018, 288, 782-790.	3.6	47
92	Prevalent osteoporotic vertebral fractures more likely involve the upper endplate than the lower endplate and even more so in males. Annals of Translational Medicine, 2018, 6, 442-442.	0.7	22
93	Informed communication with study subjects of radiographically detected osteoporotic vertebral deformity. Quantitative Imaging in Medicine and Surgery, 2018, 8, 876-880.	1.1	14
94	Topical Application of Mesenchymal Stromal Cells Ameliorated Liver Parenchyma Damage After Ischemia-Reperfusion Injury in an Animal Model. Transplantation Direct, 2017, 3, e160.	0.8	5
95	Ultra-high loading of sinoporphyrin sodium in ferritin for single-wave motivated photothermal and photodynamic co-therapy. Biomaterials Science, 2017, 5, 1512-1516.	2.6	40
96	Bi-phase age-related brain gray matter magnetic resonance T1ï•relaxation time change in adults. Magnetic Resonance Imaging, 2017, 39, 200-205.	1.0	13
97	Lumbar degenerative spondylolisthesis epidemiology: A systematic review with a focus on gender-specific and age-specific prevalence. Journal of Orthopaedic Translation, 2017, 11, 39-52.	1.9	114
98	Multifunctional biohybrid magnetite microrobots for imaging-guided therapy. Science Robotics, 2017, 2, .	9.9	594
99	Hedgehog signaling in bone regulates whole-body energy metabolism through a bone–adipose endocrine relay mediated by PTHrP and adiponectin. Cell Death and Differentiation, 2017, 24, 225-237.	5.0	19
100	On Magnetic Resonance Imaging of Intervertebral Disc Aging. Sports Medicine, 2017, 47, 187-188.	3.1	5
101	Menopause as a potential cause for higher prevalence of low back pain in women than in age-matched men. Journal of Orthopaedic Translation, 2017, 8, 1-4.	1.9	32
102	A comprehensive literatures update of clinical researches of superparamagnetic resonance iron oxide nanoparticles for magnetic resonance imaging. Quantitative Imaging in Medicine and Surgery, 2017, 7, 88-122.	1.1	177
103	How liver pathologies contribute to T1rho contrast require more careful studies. Quantitative Imaging in Medicine and Surgery, 2017, 7, 608-613.	1.1	15
104	Preface to 2017 focused issue: Quantitative Imaging of Thoracic Diseases. Journal of Thoracic Disease, 2017, 9, 4723-4723.	0.6	0
105	Identifying osteoporotic vertebral endplate and cortex fractures. Quantitative Imaging in Medicine and Surgery, 2017, 7, 555-591.	1.1	67
106	Liver intravoxel incoherent motion (IVIM) magnetic resonance imaging: a comprehensive review of published data on normal values and applications for fibrosis and tumor evaluation. Quantitative Imaging in Medicine and Surgery, 2017, 7, 59-78.	1.1	113
107	Primary thyroid lymphoma: CT findings of a rare malignant tumor with pathologic correlations. Translational Cancer Research, 2017, 6, 578-587.	0.4	3
108	Preface to 2017 focused issue: Translational Imaging in Cancer Patient Care. Translational Cancer Research, 2017, 6, 1028-1031.	0.4	0

#	Article	IF	CITATIONS
109	Intra-arterial delivery of superparamagnetic iron-oxide nanoshell and polyvinyl alcohol based chemoembolization system for the treatment of liver tumor. Discovery Medicine, 2017, 23, 27-39.	0.5	9
110	Gender Differences in Regional Brain Activity in Patients with Chronic Primary Insomnia: Evidence from a Resting-State fMRI Study. Journal of Clinical Sleep Medicine, 2016, 12, 363-374.	1.4	94
111	A higher aneurysmal subarachnoid hemorrhage incidence in women prior to menopause: a retrospective analysis of 4,895 cases from eight hospitals in China. Quantitative Imaging in Medicine and Surgery, 2016, 6, 151-156.	1.1	19
112	Will the science and technology gap between China and USA becomes narrower, wider, or stay in the same in 50 years' time?. Quantitative Imaging in Medicine and Surgery, 2016, 6, 233-237.	1.1	1
113	South Korean degenerative spondylolisthesis patients had surgical treatment at earlier age than Japanese, American, and European patients: a published literature observation. Quantitative Imaging in Medicine and Surgery, 2016, 6, 785-790.	1.1	6
114	Breath-hold black blood quantitative T1rho imaging of liver using single shot fast spin echo acquisition. Quantitative Imaging in Medicine and Surgery, 2016, 6, 168-177.	1.1	26
115	Systemic review and meta-analysis of diagnostic imaging technologies. Quantitative Imaging in Medicine and Surgery, 2016, 6, 615-618.	1.1	4
116	Towards consistency for magnetic resonance (MR) relaxometry of lumbar intervertebral discs. Quantitative Imaging in Medicine and Surgery, 2016, 6, 474-477.	1.1	5
117	Black blood T1rho MR imaging may diagnose early stage liver fibrosis: a proof-of-principle study with rat biliary duct ligation model. Quantitative Imaging in Medicine and Surgery, 2016, 6, 353-363.	1.1	24
118	Improvement in the Detection of Cystic Metastatic Papillary Thyroid Carcinoma by Measurement of Thyroglobulin in Aspirated Fluid. BioMed Research International, 2016, 2016, 1-6.	0.9	6
119	Increased low back pain prevalence in females than in males after menopause age: evidences based on synthetic literature review. Quantitative Imaging in Medicine and Surgery, 2016, 6, 199-206.	1.1	157
120	Magnetic resonance imaging of retroperitoneal interfascial plane involvement in acute pancreatitis. Quantitative Imaging in Medicine and Surgery, 2016, 6, 250-258.	1.1	9
121	Lumbar Spondylolisthesis Progression and De Novo Spondylolisthesis in Elderly Chinese Men and Women. Spine, 2016, 41, 1096-1103.	1.0	32
122	Melamine Impairs Renal and Vascular Function in Rats. Scientific Reports, 2016, 6, 28041.	1.6	10
123	Chemical Exchange Saturation Transfer (CEST) MR Technique for Liver Imaging at 3.0 Tesla: an Evaluation of Different Offset Number and an After-Meal and Over-Night-Fast Comparison. Molecular Imaging and Biology, 2016, 18, 274-282.	1.3	27
124	T1ϕrelaxation time in brain regions increases with ageing: an experimental MRI observation in rats. British Journal of Radiology, 2016, 89, 20140704.	1.0	10
125	Comparison of three approaches for definingÂnucleus pulposus and annulus fibrosus on sagittal magnetic resonance images of the lumbar spine. Journal of Orthopaedic Translation, 2016, 6, 34-41.	1.9	14
126	Superparamagnetic Iron Oxide Nanoparticles for Cellular Imaging and Targeted Therapy: Opportunities		1

and Challenges for Clinical Translation. , 2016, , 29-51.

#	Article	IF	CITATIONS
127	Myocardial <i>T</i> ₁ rho mapping of patients with endâ€stage renal disease and its comparison with <i>T</i> ₁ mapping and <i>T</i> ₂ mapping: A feasibility and reproducibility study. Journal of Magnetic Resonance Imaging, 2016, 44, 723-731.	1.9	25
128	Bilateral Common Carotid Artery Occlusion in Spontaneously Hypertensive Rats: A Feasible Animal Model for Ocular Ischemic Syndrome. Anatomical Record, 2016, 299, 806-814.	0.8	4
129	Imaging-guided delivery of RNAi for anticancer treatment. Advanced Drug Delivery Reviews, 2016, 104, 44-60.	6.6	102
130	High Serum SHBC Predicts Incident Vertebral Fractures in Elderly Men. Journal of Bone and Mineral Research, 2016, 31, 683-689.	3.1	38
131	Chemical exchange saturation transfer (CEST) MR technique for in-vivo liver imaging at 3.0 tesla. European Radiology, 2016, 26, 1792-1800.	2.3	19
132	Using Gelatin Nanoparticle Mediated Intranasal Delivery of Neuropeptide Substance P to Enhance Neuro-Recovery in Hemiparkinsonian Rats. PLoS ONE, 2016, 11, e0148848.	1.1	38
133	Contrast enhanced ultrasound guided biopsy shows higher positive sampling rate than conventional ultrasound guided biopsy for gastrointestinal stromal tumors diagnosis. Translational Cancer Research, 2016, 5, 152-159.	0.4	2
134	Evaluation of Glycosaminoglycan in the Lumbar Disc Using Chemical Exchange Saturation Transfer MR at 3.0 Tesla: Reproducibility and Correlation with Disc Degeneration. Biomedical and Environmental Sciences, 2016, 29, 47-55.	0.2	8
135	AME survey-003 A2: on the attractiveness of an medicine career in current China with a survey of 7,508 medical professionals and 443 non-medical professionals. Quantitative Imaging in Medicine and Surgery, 2016, 6, 84-102.	1.1	6
136	Biomedical imaging in translational orthopaedic research. Journal of Orthopaedic Translation, 2015, 3, 157-159.	1.9	2
137	InÂvivo three-dimensional magnetic resonance imaging of rat knee osteoarthritis model induced using meniscal transection. Journal of Orthopaedic Translation, 2015, 3, 134-141.	1.9	8
138	Postmenopausal Chinese women show accelerated lumbar disc degeneration compared with Chinese men. Journal of Orthopaedic Translation, 2015, 3, 205-211.	1.9	36
139	Metal–Organic Frameworkâ€Based Nanomedicine Platforms for Drug Delivery and Molecular Imaging. Small, 2015, 11, 4806-4822.	5.2	375
140	Blockage of Src by Specific siRNA as a Novel Therapeutic Strategy to Prevent Destructive Repair in Steroid-Associated Osteonecrosis in Rabbits. Journal of Bone and Mineral Research, 2015, 30, 2044-2057.	3.1	26
141	Rapid Increase in Marrow Fat Content and Decrease in Marrow Perfusion in Lumbar Vertebra Following Bilateral Oophorectomy: An MR Imaging-Based Prospective Longitudinal Study. Korean Journal of Radiology, 2015, 16, 154.	1.5	19
142	Current status of superparamagnetic iron oxide contrast agents for liver magnetic resonance imaging. World Journal of Gastroenterology, 2015, 21, 13400.	1.4	185
143	Epidemiological investigation of 264 sporadic cases of ruptured cerebral aneurysm at a single institution in southwest China. Neuropsychiatric Disease and Treatment, 2015, 11, 1609.	1.0	7
144	PANDA‶1]: Integrating principal component analysis and dictionary learning for fast T1I-mapping. Magnetic Resonance in Medicine, 2015, 73, 263-272.	1.9	40

#	Article	IF	CITATIONS
145	Curcumin-conjugated magnetic nanoparticles for detecting amyloid plaques in Alzheimer's disease mice using magnetic resonance imaging (MRI). Biomaterials, 2015, 44, 155-172.	5.7	240
146	Synthesis of Absorption-Dominant Small Gold Nanorods and Their Plasmonic Properties. Langmuir, 2015, 31, 7418-7426.	1.6	76
147	Long-term total sleep deprivation decreases the default spontaneous activity and connectivity pattern in healthy male subjects: a resting-state fMRI study. Neuropsychiatric Disease and Treatment, 2015, 11, 761.	1.0	95
148	High Performance Photoluminescent Carbon Dots for In Vitro and In Vivo Bioimaging: Effect of Nitrogen Doping Ratios. Langmuir, 2015, 31, 8063-8073.	1.6	175
149	Src inhibitor reduces permeability without disturbing vascularization and prevents bone destruction in steroid-associated osteonecrotic lesions in rabbits. Scientific Reports, 2015, 5, 8856.	1.6	6
150	Continued progression of lumbar disc degeneration in postmenopausal women. Climacteric, 2015, 18, 435-435.	1.1	10
151	Scientific and industrial challenges of developing nanoparticle-based theranostics and multiple-modality contrast agents for clinical application. Nanoscale, 2015, 7, 16146-16150.	2.8	24
152	Disorder enhanced conductance in graphene. Physica B: Condensed Matter, 2015, 478, 84-88.	1.3	4
153	Application of Molecular Imaging Technologies in Antitumor Drug Development and Therapy. Current Pharmaceutical Design, 2015, 21, 2136-2146.	0.9	8
154	Opportunities and Challenges of Fluorescent Carbon Dots in Translational Optical Imaging. Current Pharmaceutical Design, 2015, 21, 5401-5416.	0.9	61
155	Transcatheter embolization therapy in liver cancer: an update of clinical evidences. Chinese Journal of Cancer Research: Official Journal of China Anti-Cancer Association, Beijing Institute for Cancer Research, 2015, 27, 96-121.	0.7	67
156	Exponential growth of publications on carbon nanodots by Chinese authors. Journal of Thoracic Disease, 2015, 7, E201-5.	0.6	10
157	Evaluation of biocompatible alginate- and deferoxamine-coated ternary composites for magnetic resonance imaging and gene delivery into glioblastoma cells. Quantitative Imaging in Medicine and Surgery, 2015, 5, 382-91.	1.1	5
158	Total gadolinium tissue deposition and skin structural findings following the administration of structurally different gadolinium chelates in healthy and ovariectomized female rats. Quantitative Imaging in Medicine and Surgery, 2015, 5, 534-45.	1.1	29
159	Recent advances in surgical planning & navigation for tumor biopsy and resection. Quantitative Imaging in Medicine and Surgery, 2015, 5, 640-8.	1.1	10
160	AME survey-003 A1-part 2: the motivation factors of medical doctors in China. Quantitative Imaging in Medicine and Surgery, 2015, 5, 917-24.	1.1	10
161	Late postpartum eclampsia complicated with posterior reversible encephalopathy syndrome: a case report and a literature review. Quantitative Imaging in Medicine and Surgery, 2015, 5, 909-16.	1.1	21
162	T1ϕmagnetic resonance: basic physics principles and applications in knee and intervertebral disc imaging. Quantitative Imaging in Medicine and Surgery, 2015, 5, 858-85.	1.1	62

#	Article	IF	CITATIONS
163	Double contrast percutaneous transhepatic cholangiographic CT in patients with obstructive jaundice: an initial experience of 7 cases Journal of the Belgian Society of Radiology, 2015, 95, 251.	0.2	2
164	On the training of young doctors in China. Quantitative Imaging in Medicine and Surgery, 2015, 5, 182-5.	1.1	8
165	English language usage pattern in China mainland doctors: AME survey-001 initial analysis results. Quantitative Imaging in Medicine and Surgery, 2015, 5, 174-81.	1.1	16
166	Physical scientists research biomedicine: a call for caution. Chinese Journal of Cancer Research: Official Journal of China Anti-Cancer Association, Beijing Institute for Cancer Research, 2015, 27, 94-5.	0.7	9
167	A long way ahead to improve the cost-effectiveness of biomedical research in China. Journal of Thoracic Disease, 2015, 7, E62-4.	0.6	5
168	Why so many Chinese clinical doctors are competing for basic research grants?. Quantitative Imaging in Medicine and Surgery, 2015, 5, 489-90.	1.1	2
169	Top five medical innovations in China mainland since Xinhai revolution [1911]: results of AME survey-002. Quantitative Imaging in Medicine and Surgery, 2015, 5, 453-66.	1.1	12
170	Why China is currently underperforming in medical innovation and what China can do about it?-Part II. Quantitative Imaging in Medicine and Surgery, 2015, 5, 335-9.	1.1	3
171	Why China is currently underperforming in medical innovation and what China can do about it?-Part I. Quantitative Imaging in Medicine and Surgery, 2015, 5, 332-4.	1.1	5
172	Income of medical doctors in Germany. Quantitative Imaging in Medicine and Surgery, 2015, 5, 488.	1.1	2
173	Why China is currently underperforming in medical innovation and what China can do about it?-Part III: social psychology and evolutionary psychology perspectives. Quantitative Imaging in Medicine and Surgery, 2015, 5, 494-502.	1.1	1
174	On pancreatic cancer screening by magnetic resonance imaging with the recent evidence by Del Chiaro and colleagues. Chinese Journal of Cancer Research: Official Journal of China Anti-Cancer Association, Beijing Institute for Cancer Research, 2015, 27, 417-22.	0.7	1
175	AME survey-003 A1-part1: in current China, do you regret you joined the medical profession. Quantitative Imaging in Medicine and Surgery, 2015, 5, 765-73.	1.1	7
176	The role of Chaoyang People's Hospital for the development of trioxide as an effective treatment for acute promyelocytic leukemia treatment. Quantitative Imaging in Medicine and Surgery, 2015, 5, 791.	1.1	0
177	Non-Gaussian Analysis of Diffusion Weighted Imaging in Head and Neck at 3T: A Pilot Study in Patients with Nasopharyngeal Carcinoma. PLoS ONE, 2014, 9, e87024.	1.1	72
178	Time-Efficient Myocardial Contrast Partition Coefficient Measurement from Early Enhancement with Magnetic Resonance Imaging. PLoS ONE, 2014, 9, e93124.	1.1	5
179	Time-Intensity Curve Parameters in Rectal Cancer Measured Using Endorectal Ultrasonography with Sterile Coupling Gels Filling the Rectum: Correlations with Tumor Angiogenesis and Clinicopathological Features. BioMed Research International, 2014, 2014, 1-7.	0.9	22
180	Molecular Imaging: From Bench to Clinic. BioMed Research International, 2014, 2014, 1-3.	0.9	16

#	Article	IF	CITATIONS
181	New Progress in Angiogenesis Therapy of Cardiovascular Disease by Ultrasound Targeted Microbubble Destruction. BioMed Research International, 2014, 2014, 1-12.	0.9	37
182	Hepatic Sinusoidal Obstruction Syndrome Caused by Herbal Medicine: CT and MRI Features. Korean Journal of Radiology, 2014, 15, 218.	1.5	67
183	Altered intrinsic regional brain spontaneous activity and subjective sleep quality in patients with chronic primary insomnia: a resting-state fMRI study. Neuropsychiatric Disease and Treatment, 2014, 10, 2163.	1.0	115
184	Cerebellar cryptococcosis characterized by a space-occupying lesion in an immunocompetent non-HIV patient. Neuropsychiatric Disease and Treatment, 2014, 11, 21.	1.0	6
185	Ultrasound-Mediated Local Drug and Gene Delivery Using Nanocarriers. BioMed Research International, 2014, 2014, 1-13.	0.9	66
186	Acoustic Radiation Force Impulse Elastography for Efficacy Evaluation after Hepatocellular Carcinoma Radiofrequency Ablation: A Comparative Study with Contrast-Enhanced Ultrasound. BioMed Research International, 2014, 2014, 1-7.	0.9	13
187	New Researches and Application Progress of Commonly Used Optical Molecular Imaging Technology. BioMed Research International, 2014, 2014, 1-22.	0.9	7
188	Advance of Molecular Imaging Technology and Targeted Imaging Agent in Imaging and Therapy. BioMed Research International, 2014, 2014, 1-12.	0.9	90
189	Automatic detection of arterial input function in dynamic contrast enhanced MRI based on affinity propagation clustering. Journal of Magnetic Resonance Imaging, 2014, 39, spcone-spcone.	1.9	1
190	Inâ€Vivo Chemoembolization and Magnetic Resonance Imaging of Liver Tumors by Using Iron Oxide Nanoshell/Doxorubicin/Poly(vinyl alcohol) Hybrid Composites. Angewandte Chemie - International Edition, 2014, 53, 4812-4815.	7.2	47
191	Evaluation of Disease Stage of Radiation-Induced Brain Injury: a DTI Study with Pathological Correlation. Applied Magnetic Resonance, 2014, 45, 427-436.	0.6	Ο
192	Prevalence and risk factors of lumbar spondylolisthesis in elderly Chinese men and women. European Radiology, 2014, 24, 441-448.	2.3	64
193	Automatic Tuberculosis Screening Using Chest Radiographs. IEEE Transactions on Medical Imaging, 2014, 33, 233-245.	5.4	403
194	Amide proton transferâ€weighted imaging of the head and neck at 3 T: a feasibility study on healthy human subjects and patients with head and neck cancer. NMR in Biomedicine, 2014, 27, 1239-1247.	1.6	57
195	Automatic detection of arterial input function in dynamic contrast enhanced MRI based on affinity propagation clustering. Journal of Magnetic Resonance Imaging, 2014, 39, 1327-1337.	1.9	23
196	Improving intra-voxel incoherent motion MRI quantification using wild bootstrap. , 2014, , .		1
197	Cellular uptake behaviour, photothermal therapy performance, and cytotoxicity of gold nanorods with various coatings. Nanoscale, 2014, 6, 11462-11472.	2.8	92
198	CT features of focal organizing pneumonia: An analysis of consecutive histopathologically confirmed 45 cases. European Journal of Radiology, 2014, 83, 73-78.	1.2	38

Yì XIÃING J WÃING

#	ARTICLE	IF	CITATIONS
199	Comparative study of poly (lactic-co-glycolic acid)/tricalcium phosphate scaffolds incorporated or coated with osteogenic growth factors for enhancement of bone regeneration. Journal of Orthopaedic Translation, 2014, 2, 91-104.	1.9	28
200	Improved quantification of chemical exchange saturation transfer (CEST) MRI using nonlocal means. , 2014, , .		1
201	An Analysis of 1256 Cases of Sporadic Ruptured Cerebral Aneurysm in a Single Chinese Institution. PLoS ONE, 2014, 9, e85668.	1.1	38
202	Abdominal Regional Fat Distribution on MRI Correlates with Cholecystolithiasis. PLoS ONE, 2014, 9, e109776.	1.1	4
203	Decreases in Molecular Diffusion, Perfusion Fraction and Perfusion-Related Diffusion in Fibrotic Livers: A Prospective Clinical Intravoxel Incoherent Motion MR Imaging Study. PLoS ONE, 2014, 9, e113846.	1.1	43
204	Evidence based imaging strategies for solitary pulmonary nodule. Journal of Thoracic Disease, 2014, 6, 872-87.	0.6	28
205	Magnetic resonance imaging for lung cancer screen. Journal of Thoracic Disease, 2014, 6, 1340-8.	0.6	21
206	Evaluation of liver fibrosis with T1ϕMR imaging. Quantitative Imaging in Medicine and Surgery, 2014, 4, 152-5.	1.1	31
207	Age related reduction of T1rho and T2 magnetic resonance relaxation times of lumbar intervertebral disc. Quantitative Imaging in Medicine and Surgery, 2014, 4, 259-64.	1.1	30
208	Implications of Web of Science journal impact factor for scientific output evaluation in 16 institutions and investigators' opinion. Quantitative Imaging in Medicine and Surgery, 2014, 4, 453-61.	1.1	23
209	Two public chest X-ray datasets for computer-aided screening of pulmonary diseases. Quantitative Imaging in Medicine and Surgery, 2014, 4, 475-7.	1.1	370
210	Focus on China: should clinicians engage in research? and lessons from other countries. Quantitative Imaging in Medicine and Surgery, 2014, 4, 413-25.	1.1	18
211	Comment on: Zhang Z, et al. Focus on China: should clinicians engage in research? and lessons from other countries. Quant Imaging Med Surg 2014;4:413-25. Quantitative Imaging in Medicine and Surgery, 2014, 4, 430-2.	1.1	5
212	Introduce fair competition mechanism in China healthcare system. Quantitative Imaging in Medicine and Surgery, 2014, 4, 498-9.	1.1	5
213	Relative income of clinical faculty members vs. science faculty members in university settings-a short survey of France, Hong Kong, India, Japan, South Korea, The Netherlands, Taiwan, UK, and USA. Quantitative Imaging in Medicine and Surgery, 2014, 4, 500-1.	1.1	6
214	Advance modern medicine with clinical case reports. Quantitative Imaging in Medicine and Surgery, 2014, 4, 439-43.	1.1	12
215	Inner annulus fibrosus in non-degenerated intervertebral disc shows bright signal on T2 weighted MR image. Quantitative Imaging in Medicine and Surgery, 2014, 4, 504.	1.1	3
216	CT and MR features of xanthogranulomatous cholecystitis: An analysis of consecutive 49 cases. European Journal of Radiology, 2013, 82, 1391-1397.	1.2	55

#	Article	IF	CITATIONS
217	Organic Nitrate Maintains Bone Marrow Blood Perfusion in Ovariectomized Female Rats: A Dynamic, Contrast-Enhanced Magnetic Resonance Imaging (MRI) Study. Pharmaceutics, 2013, 5, 23-35.	2.0	3
218	Predictors for replanning in loco-regionally advanced nasopharyngeal carcinoma patients undergoing intensity-modulated radiation therapy: a prospective observational study. BMC Cancer, 2013, 13, 548.	1.1	18
219	PLGA/TCP composite scaffold incorporating bioactive phytomolecule icaritin for enhancement of bone defect repair in rabbits. Acta Biomaterialia, 2013, 9, 6711-6722.	4.1	84
220	Enhanced cellular uptake and gene delivery of glioblastoma with deferoxamine-coated nanoparticle/plasmid DNA/branched polyethylenimine composites. Chemical Communications, 2013, 49, 549-551.	2.2	22
221	T1rho and T2 relaxation times for lumbar disc degeneration: an in vivo comparative study at 3.0-Tesla MRI. European Radiology, 2013, 23, 228-234.	2.3	76
222	Nanoparticle–DNA–polymer composites for hepatocellular carcinoma cell labeling, sensing, and magnetic resonance imaging. Methods, 2013, 64, 315-321.	1.9	14
223	Prevalence and risk factors of radiographic vertebral fractures in elderly Chinese men and women: results of Mr. OS (Hong Kong) and Ms. OS (Hong Kong) studies. Osteoporosis International, 2013, 24, 877-885.	1.3	94
224	Folate-conjugated Fe3O4@SiO2@gold nanorods@mesoporous SiO2 hybrid nanomaterial: a theranostic agent for magnetic resonance imaging and photothermal therapy. Journal of Materials Chemistry B, 2013, 1, 2934.	2.9	72
225	Ultrasound, pH, and Magnetically Responsive Crown-Ether-Coated Core/Shell Nanoparticles as Drug Encapsulation and Release Systems. ACS Applied Materials & Interfaces, 2013, 5, 1566-1574.	4.0	122
226	Increased Efficacies in Magnetofection and Gene Delivery to Hepatocellular Carcinoma Cells with Ternary Organic–Inorganic Hybrid Nanocomposites. Chemistry - an Asian Journal, 2013, 8, 1760-1764.	1.7	13
227	Calcitriol restores renovascular function in estrogen-deficient rats through downregulation of cyclooxygenase-2 and the thromboxane-prostanoid receptor. Kidney International, 2013, 84, 54-63.	2.6	30
228	Prevalence and Sex Difference of Lumbar Disc Space Narrowing in Elderly Chinese Men and Women: Osteoporotic Fractures in Men (Hong Kong) and Osteoporotic Fractures in Women (Hong Kong) Studies. Arthritis and Rheumatism, 2013, 65, 1004-1010.	6.7	66
229	The volumetric relationship of white matter lesion and contrast-enhanced lesion in delayed radiation brain injury: an MRI-based study. British Journal of Neurosurgery, 2013, 27, 662-667.	0.4	1
230	Terahertz time domain spectroscopy of rat skin tissues. , 2013, , .		0
231	Accuracy and uncertainty of asymmetric magnetization transfer ratio quantification for amide proton transfer (APT) imaging at 3T: A Monte Carlo study. , 2013, 2013, 5139-42.		5
232	Cramér-Rao bound for Intravoxel Incoherent Motion Diffusion Weighted Imaging fitting. , 2013, 2013, 511-4.		21
233	TO THE EDITOR. Spine, 2013, 38, 201.	1.0	0
234	Recent Advances in Superparamagnetic Iron Oxide Nanoparticles for Cellular Imaging and Targeted Therapy Research. Current Pharmaceutical Design, 2013, 19, 6575-6593.	0.9	102

#	Article	IF	CITATIONS
235	Fatal bleeding in a nasopharyngeal carcinoma patient after concurrent chemoradiation plus cetuximab: a case report. OncoTargets and Therapy, 2013, 6, 703.	1.0	8
236	Quantitative Imaging in Medicine and Surgery: progress & perspective. Quantitative Imaging in Medicine and Surgery, 2013, 3, 1-4.	1.1	5
237	Accelerated T1rho relaxation quantification in intervertebral disc using limited spin-lock times. Quantitative Imaging in Medicine and Surgery, 2013, 3, 54-8.	1.1	13
238	Ternary hybrid nanocomposites for gene delivery and magnetic resonance imaging of hepatocellular carcinoma cells. Quantitative Imaging in Medicine and Surgery, 2013, 3, 302-7.	1.1	9
239	Further exploration of MRI techniques for liver T1rho quantification. Quantitative Imaging in Medicine and Surgery, 2013, 3, 308-15.	1.1	12
240	MR chemical exchange imaging with spin-lock technique (CESL): a theoretical analysis of the Z-spectrum using a two-pool <i>R</i> _{1Ï} relaxation model beyond the fast-exchange limit. Physics in Medicine and Biology, 2012, 57, 8185-8200.	1.6	26
241	DL-3-n-Butylphthalide, an Anti-Oxidant Agent, Prevents Neurological Deficits and Cerebral Injury Following Stroke per Functional Analysis, Magnetic Resonance Imaging and Histological Assessment. Current Neurovascular Research, 2012, 9, 167-175.	0.4	34
242	Vertebral body corner oedema <i>vs</i> gadolinium enhancement as biomarkers of active spinal inflammation in ankylosing spondylitis. British Journal of Radiology, 2012, 85, e702-e708.	1.0	5
243	Compromised perfusion in femoral head in normal rats: distinctive perfusion MRI evidence of contrast washout delay. British Journal of Radiology, 2012, 85, e436-e441.	1.0	8
244	CT and Ultrasound Features of Basal Cell Adenoma of the Parotid Gland: A Report of 22 Cases with Pathologic Correlation. American Journal of Neuroradiology, 2012, 33, 434-438.	1.2	20
245	Observation of bi-exponential T _{1Ï} relaxation of <i>in-vivo</i> rat muscles at 3T. Acta Radiologica, 2012, 53, 675-681.	0.5	20
246	Quantification of <i>T</i> _{1Ï} relaxation by using rotary echo spin-lock pulses in the presence of <i>B</i> ₀ inhomogeneity. Physics in Medicine and Biology, 2012, 57, 5003-5016.	1.6	15
247	Optimized efficient liver <i>T</i> _{1Ï} mapping using limited spin lock times. Physics in Medicine and Biology, 2012, 57, 1631-1640.	1.6	27
248	Liver <i>T</i> ₁ <i>Ï</i> MRI measurement in healthy human subjects at 3 T: a preliminary study with a two-dimensional fast-field echo sequence. British Journal of Radiology, 2012, 85, e590-e595.	1.0	46
249	Morphological Changes of Lumbar Vertebral Bodies and Intervertebral Discs Associated With Decrease in Bone Mineral Density of the Spine. Spine, 2012, 37, E1415-E1421.	1.0	29
250	Dipeptidyl Peptidase 4 Inhibitor Sitagliptin Protects Endothelial Function in Hypertension Through a Glucagon–Like Peptide 1–Dependent Mechanism. Hypertension, 2012, 60, 833-841.	1.3	164
251	Ultrasound Findings of Papillary Thyroid Microcarcinoma: AÂReview of 113 Consecutive Cases with Histopathologic Correlation. Ultrasound in Medicine and Biology, 2012, 38, 1681-1688.	0.7	37
252	Radiotherapy for Nasopharyngeal Carcinoma and Combined Capecitabine and Nimotuzumab Treatment for Lung Metastases in a Liver Transplantation Recipient: A Case Experience of Sustained Complete Response. Cancer Biotherapy and Radiopharmaceuticals, 2012, 27, 519-523.	0.7	9

#	Article	IF	CITATIONS
253	Perfusion study on Modic changes of spine based on DCE-MRI. , 2012, , .		1
254	Hollow superparamagnetic iron oxide nanoshells as a hydrophobic anticancer drug carrier: intracelluar pH-dependent drug release and enhanced cytotoxicity. Nanoscale, 2012, 4, 5744.	2.8	65
255	Study of magnetization evolution by using composite spin-lock pulses for T <inf>1ρ</inf> imaging. , 2012, 2012, 408-11.		3
256	Gender differences in brain regional homogeneity of healthy subjects after normal sleep and after sleep and after sleep deprivation: A resting-state fMRI study. Sleep Medicine, 2012, 13, 720-727.	0.8	124
257	A delivery system targeting bone formation surfaces to facilitate RNAi-based anabolic therapy. Nature Medicine, 2012, 18, 307-314.	15.2	354
258	Mapping the central effects of chronic ketamine administration in an adolescent primate model by functional magnetic resonance imaging (fMRI). NeuroToxicology, 2012, 33, 70-77.	1.4	45
259	Computerized quantification of bone tissue and marrow in stained microscopic images. Cytometry Part A: the Journal of the International Society for Analytical Cytology, 2012, 81A, 916-921.	1.1	5
260	Enhanced cellular uptake of aminosilane-coated superparamagnetic iron oxide nanoparticles in mammalian cell lines. International Journal of Nanomedicine, 2012, 7, 953.	3.3	81
261	Photocytotoxicity and Magnetic Relaxivity Responses of Dual-Porous γ-Fe ₂ 0 ₃ @ <i>meso</i> -SiO ₂ Microspheres. ACS Applied Materials & Interfaces, 2012, 4, 2033-2040.	4.0	51
262	Oxidative Stress-Dependent Cyclooxygenase-2-Derived Prostaglandin F _{2α} Impairs Endothelial Function in Renovascular Hypertensive Rats. Antioxidants and Redox Signaling, 2012, 16, 363-373.	2.5	77
263	lcaritin, an Exogenous Phytomolecule, Enhances Osteogenesis but Not Angiogenesis—An In Vitro Efficacy Study. PLoS ONE, 2012, 7, e41264.	1.1	46
264	Experimental Evaluation of Accelerated T1rho Relaxation Quantification in Human Liver Using Limited Spin-Lock Times. Korean Journal of Radiology, 2012, 13, 736.	1.5	30
265	MR T1ϕas an imaging biomarker for monitoring liver injury progression and regression: an experimental study in rats with carbon tetrachloride intoxication. European Radiology, 2012, 22, 1709-1716.	2.3	56
266	Ultra-fast method to synthesize mesoporous magnetite nanoclusters as highly sensitive magnetic resonance probe. Journal of Colloid and Interface Science, 2012, 379, 1-7.	5.0	21
267	Effect of ovariectomy on contrast agent diffusion into lumbar intervertebral disc: a dynamic contrast-enhanced MRI study in female rats. Magnetic Resonance Imaging, 2012, 30, 683-688.	1.0	21
268	Relationship between respiratory viral load and lung lesion severity: a study in 24 cases of pandemic H1N1 2009 influenza A pneumonia. Journal of Thoracic Disease, 2012, 4, 377-83.	0.6	6
269	Carbon coated superparamagnetic iron oxide nanoparticles for sentinel lymph nodes mapping. Quantitative Imaging in Medicine and Surgery, 2012, 2, 53-6.	1.1	20
270	Characteristics of rat lumbar vertebral body bone mineral density and differential segmental responses to sex hormone deficiency: a clinical multidetector computed tomography study. Biomedical and Environmental Sciences, 2012, 25, 607-13.	0.2	7

#	Article	IF	CITATIONS
271	Synthesis of Biocompatible, Mesoporous Fe ₃ O ₄ Nano/Microspheres with Large Surface Area for Magnetic Resonance Imaging and Therapeutic Applications. ACS Applied Materials & Interfaces, 2011, 3, 237-244.	4.0	197
272	A promising diagnostic method: Terahertz pulsed imaging and spectroscopy. World Journal of Radiology, 2011, 3, 55.	0.5	100
273	Menopause causes vertebral endplate degeneration and decrease in nutrient diffusion to the intervertebral discs. Medical Hypotheses, 2011, 77, 18-20.	0.8	41
274	Chemoembolization agents for cancer treatment. European Journal of Pharmaceutical Sciences, 2011, 44, 1-10.	1.9	61
275	Radiological findings of renal leiomyomas: a report of five surgically confirmed cases. Abdominal Imaging, 2011, 36, 604-608.	2.0	6
276	Enhanced Ablation of High Intensity Focused Ultrasound with Microbubbles: An Experimental Study on Rabbit Hepatic VX2 Tumors. CardioVascular and Interventional Radiology, 2011, 34, 1050-1057.	0.9	18
277	Relationship between gender, bone mineral density, and disc degeneration in the lumbar spine: a study in elderly subjects using an eight-level MRI-based disc degeneration grading system. Osteoporosis International, 2011, 22, 91-96.	1.3	89
278	Relationship between hip bone mineral density and lumbar disc degeneration: A study in elderly subjects using an eightâ€level MRIâ€based disc degeneration grading system. Journal of Magnetic Resonance Imaging, 2011, 33, 916-920.	1.9	24
279	Color quantification for evaluation of stained tissues. Cytometry Part A: the Journal of the International Society for Analytical Cytology, 2011, 79A, 311-316.	1.1	7
280	T1ϕMR Imaging Is Sensitive to Evaluate Liver Fibrosis: An Experimental Study in a Rat Biliary Duct Ligation Model. Radiology, 2011, 259, 712-719.	3.6	121
281	Frameless stereotactic aspiration and subsequent fibrinolytic therapy for the treatment of spontaneous intracerebral haemorrhage. British Journal of Neurosurgery, 2011, 25, 369-375.	0.4	20
282	Efficacy and Durability in Direct Labeling of Mesenchymal Stem Cells Using Ultrasmall Superparamagnetic Iron Oxide Nanoparticles with Organosilica, Dextran, and PEG Coatings. Materials, 2011, 4, 703-715.	1.3	27
283	Superparamagnetic iron oxide based MRI contrast agents: Current status of clinical application. Quantitative Imaging in Medicine and Surgery, 2011, 1, 35-40.	1.1	636
284	The impact of quantitative imaging in medicine and surgery: Charting our course for the future. Quantitative Imaging in Medicine and Surgery, 2011, 1, 1-3.	1.1	64
285	Facile synthesis of size-controllable monodispersed ferrite nanospheres. Journal of Materials Chemistry, 2010, 20, 5086.	6.7	197
286	Hemorrhage of brain metastasis from non-small cell lung cancer post gefitinib therapy: two case reports and review of the literature. BMC Cancer, 2010, 10, 49.	1.1	20
287	Lowâ€intensity pulsed ultrasound increases cellular uptake of superparamagnetic iron oxide nanomaterial: Results from human osteosarcoma cell line U2OS. Journal of Magnetic Resonance Imaging, 2010, 31, 1508-1513.	1.9	27
288	Concatenated and parallel optimization for the estimation of <i>T</i> ₁ map in FLASH MRI with multiple flip angles. Magnetic Resonance in Medicine, 2010, 63, 1431-1436.	1.9	8

#	Article	IF	CITATIONS
289	Small Field-Of-View Surface Coil MR Imaging of Talar Osteochondral Lesions. Foot and Ankle International, 2010, 31, 517-522.	1.1	9
290	Reduced Bone Perfusion in Osteoporosis: Likely Causes in an Ovariectomy Rat Model. Radiology, 2010, 254, 739-746.	3.6	73
291	Evolution of Radiation-induced Brain Injury: MR Imaging–based Study. Radiology, 2010, 254, 210-218.	3.6	113
292	The use of diffusion tensor tractography to measure the distance between the anterior tip of the Meyer loop and the temporal pole in a cohort from Southern China. Journal of Neurosurgery, 2010, 113, 1144-1151.	0.9	18
293	Effect of Menopause on Lumbar Disk Degeneration: Potential Etiology. Radiology, 2010, 257, 318-320.	3.6	82
294	Investigating the role of water content on the terahertz properties of rat liver cirrhosis. , 2010, , .		0
295	Activated Src phosphorylation accompanied by both vascular hyperpermeability and dominant bone resorption during destructive repair of steroid-associated osteonecrotic lesions in rabbits. Bone, 2010, 47, S401.	1.4	3
296	Higher lumbar bone mineral density is associated with narrowed intervertebral disc space, but not higher hip bone mineral density: A study in 359 elderly subjects. Bone, 2010, 47, S445.	1.4	0
297	Magnetic Nanochains of FeNi ₃ Prepared by a Template-Free Microwave-Hydrothermal Method. ACS Applied Materials & Interfaces, 2010, 2, 2579-2584.	4.0	59
298	Terahertz spectroscopy of liver cirrhosis: investigating the origin of contrast. Physics in Medicine and Biology, 2010, 55, 7587-7596.	1.6	222
299	Non-invasive MRI assessment of the articular cartilage in clinical studies and experimental settings. World Journal of Radiology, 2010, 2, 44.	0.5	25
300	Medical imaging in new drug clinical development. Journal of Thoracic Disease, 2010, 2, 245-52.	0.6	14
301	Radiological features of lung changes caused by avian influenza subtype A H5N1 virus: report of two severe adult cases with regular follow-up. Chinese Medical Journal, 2010, 123, 100-4.	0.9	15
302	An in vivo magnetic resonance imaging technique for measurement of rat lumbar vertebral body blood perfusion. Laboratory Animals, 2009, 43, 261-265.	0.5	9
303	Fossa trochanterica of the proximal femur in rabbits: An anatomic structure for potential misinterpretation on magnetic resonance images. Acta Radiologica, 2009, 50, 212-216.	0.5	6
304	Comment on Jing etÂal. original article "In vivo MR imaging tracking of magnetic iron oxide nanoparticle labeled, engineered, autologous bone marrow mesenchymal stem cells following intra-articular injection― Joint Bone Spine, 2009, 76, 118-119.	0.8	4
305	Durable Mesenchymal Stem Cell Labelling by Using Polyhedral Superparamagnetic Iron Oxide Nanoparticles. Chemistry - A European Journal, 2009, 15, 12417-12425.	1.7	59
306	Proximal femur bone marrow blood perfusion indices are reduced in hypertensive rats: A dynamic contrastâ€enhanced MRI study. Journal of Magnetic Resonance Imaging, 2009, 30, 1139-1144.	1.9	13

#	Article	IF	CITATIONS
307	Functional perfusion MRI predicts later occurrence of steroidâ€associated osteonecrosis: An experimental study in rabbits. Journal of Orthopaedic Research, 2009, 27, 742-747.	1.2	22
308	Continuous occurrence of both insufficient neovascularization and elevated vascular permeability in rabbit proximal femur during inadequate repair of steroidâ€associated osteonecrotic lesions. Arthritis and Rheumatism, 2009, 60, 2966-2977.	6.7	45
309	Rat lumbar vertebrae bone densitometry using multidetector CT. European Radiology, 2009, 19, 882-890.	2.3	11
310	Preparation, Characterization, and Catalytic Activity of Core/Shell Fe ₃ O ₄ @Polyaniline@Au Nanocomposites. Langmuir, 2009, 25, 11835-11843.	1.6	351
311	Tissue characterization using terahertz pulsed imaging in reflection geometry. Physics in Medicine and Biology, 2009, 54, 149-160.	1.6	108
312	A novel semisynthesized small molecule icaritin reduces incidence of steroid-associated osteonecrosis with inhibition of both thrombosis and lipid-deposition in a dose-dependent manner. Bone, 2009, 44, 345-356.	1.4	132
313	Reduced bone perfusion in proximal femur of subjects with decreased bone mineral density preferentially affects the femoral neck. Bone, 2009, 45, 711-715.	1.4	41
314	Tuning the Grain Size and Particle Size of Superparamagnetic Fe ₃ O ₄ Microparticles. Chemistry of Materials, 2009, 21, 5079-5087.	3.2	387
315	Biological and Magnetic Contrast Evaluation of Shape-Selective Mn–Fe Nanowires. IEEE Transactions on Nanobioscience, 2009, 8, 192-198.	2.2	26
316	Pitfalls in interpreting rat knee joint magnetic resonance images and their histological correlation. Acta Radiologica, 2009, 50, 1042-1048.	0.5	5
317	Terahertz pulsed imaging of liver cirrhosis. , 2009, , .		2
318	Vertebral blood perfusion reduction associated with vertebral bone mineral density reduction: A dynamic contrastâ€enhanced MRI study in a rat orchiectomy model. Journal of Magnetic Resonance Imaging, 2008, 28, 1515-1518.	1.9	20
319	Synthesis of Fe ₃ O ₄ @Polyaniline Core/Shell Microspheres with Well-Defined Blackberry-Like Morphology. Journal of Physical Chemistry C, 2008, 112, 18804-18809.	1.5	140
320	Bone marrow derived mesenchymal stem cell labeling using silica-coated superparamagnetic iron oxide nanoparticles: Effects of amine functional peripheries. Bone, 2008, 43, S94-S95.	1.4	2
321	Mesenchymal stem cell intracellular labeling using silica-coated superparamagnetic iron oxide nanoparticles with amine functional peripheries. , 2008, , .		5
322	Novel one-dimensional Mn—Fe oxide nanowires for cell labeling and magnetic resonance imaging. , 2008, , .		0
323	Short-term efficacy of combination methotrexate and infliximab in patients with ankylosing spondylitis: a clinical and magnetic resonance imaging correlation. Rheumatology, 2008, 47, 1358-1363.	0.9	50
324	Pitfalls in employing superparamagnetic iron oxide particles for stem cell labelling and <i>in vivo</i> MRI tracking. British Journal of Radiology, 2008, 81, 987-988.	1.0	19

#	Article	IF	CITATIONS
325	Biomedical imaging in the safety evaluation of new drugs. Laboratory Animals, 2008, 42, 433-441.	0.5	20
326	In vivo magnetic resonance imaging of animal models of knee osteoarthritis. Laboratory Animals, 2008, 42, 246-264.	0.5	26
327	Dynamic Contrast-Enhanced Magnetic Resonance Imaging of the Musculoskeletal System: Basic Principles and Clinical Applications in Bone Sarcomas and Rheumatoid Arthritis. , 2008, , 729-748.		Ο
328	Noninvasive Evaluation of Knee Cartilage Morphology by Magnetic Resonance Imaging. , 2008, , 749-769.		0
329	Characterisation of brain disorders and evaluation of therapy by functional and molecular magnetic resonance techniques. Hong Kong Medical Journal, 2008, 14, 469-78.	0.1	4
330	Modified Pfirrmann Grading System for Lumbar Intervertebral Disc Degeneration. Spine, 2007, 32, E708-E712.	1.0	367
331	Imaging Kidney in Conscious Rats with High-Frequency Ultrasound and Detection of Two Cases of Unilateral Congenital Hydronephrosis. Ultrasound in Medicine and Biology, 2007, 33, 483-486.	0.7	12
332	Whole-body three-dimensional contrast-enhanced magnetic resonance (MR) angiography with parallel imaging techniques on a multichannel MR system for the detection of various systemic arterial diseases. Heart and Vessels, 2006, 21, 395-398.	0.5	28
333	Gradient Echo MRI Characterization of Development of Atherosclerosis in the Abdominal Aorta in Watanabe Heritable Hyperlipidemic Rabbits. CardioVascular and Interventional Radiology, 2006, 29, 605-612.	0.9	9
334	N-Nitrosodiethylamine-Induced Pig Liver Hepatocellular Carcinoma Model: Radiological and Histopathological Studies. CardioVascular and Interventional Radiology, 2006, 29, 420-428.	0.9	39
335	Catheterization of the Hepatic Artery Via the Left Common Carotid Artery in Rats. CardioVascular and Interventional Radiology, 2006, 29, 1073-1076.	0.9	6
336	MRI histopathology correlation of N-phenylanthranilic acid induced nephropathy in rats. British Journal of Radiology, 2006, 79, 1009-1010.	1.0	3
337	Some aspects of rat femorotibial joint microanatomy as demonstrated by high-resolution magnetic resonance imaging. Laboratory Animals, 2006, 40, 288-295.	0.5	6
338	Fluid collection within the synovial sheath of the tendon of the flexor hallus longus muscle in the tarsal joint of rats: an anatomic variant detectable with magnetic resonance imaging. Laboratory Animals, 2006, 40, 58-62.	0.5	4
339	Vena Cava 3D Contrast-Enhanced MR Venography: A Pictorial Review. CardioVascular and Interventional Radiology, 2005, 28, 795-805.	0.9	20
340	The emerging role of medical radiologists in new drug discovery. British Journal of Radiology, 2005, 78, 1058-1058.	1.0	4
341	Medical imaging in pharmaceutical clinical trials: what radiologists should know. Clinical Radiology, 2005, 60, 1051-1057.	0.5	49
342	Mn-DPDP-enhanced 24-h delayed-scan MRI of hepatocellular carcinoma is correlated with histology. European Radiology, 2004, 14, 743-745.	2.3	4

#	Article	IF	CITATIONS
343	Effective blood signal suppression using double inversion-recovery and slice reordering for multislice fast spin-echo MRI and its application in simultaneous proton density and T2 weighted imaging. Journal of Magnetic Resonance Imaging, 2004, 20, 881-888.	1.9	13
344	3D contrast-enhanced MR portography and direct X-ray portography: a correlation study. European Radiology, 2003, 13, 1277-1285.	2.3	8
345	Atypical magnetic resonance imaging findings of craniopharyngioma. Journal of Medical Imaging and Radiation Oncology, 2001, 45, 52-57.	0.6	4
346	Superparamagnetic iron oxide contrast agents: physicochemical characteristics and applications in MR imaging. European Radiology, 2001, 11, 2319-2331.	2.3	1,247
347	Cerebral asymmetry in a selected Chinese population. Journal of Medical Imaging and Radiation Oncology, 1999, 43, 321-324.	0.6	5
348	Characterization and correction of the effects of hepatic iron on <i>T</i> _{1Ï} relaxation in the liver at 3.0T. Magnetic Resonance in Medicine, 0, , .	1.9	4